A Study of Radiation Scaling of High Enthalpy Flows in Expansion Tubes

Andreas Andrianatos [1], David Gildfind [1] and Richard Morgan [1]

[1] *Centre for Hypersonics, School of Mechanical and Mining Engineering, The University of Queensland, Brisbane, Queensland, 4072, Australia*

Abstract

During super orbital entry temperatures in the shock layer can reach up to 10,000K and at these temperatures radiative heat transfer becomes a significant contributor to the total heat flux to the surface of the vehicle. Conditions experienced during flight can be simulated in the X2 and X3 expansion tubes at the University of Queensland (UQ). Currently, high enthalpy conditions have only been simulated in X2 using small subscale models of flight vehicles and the test condition is scaled to the flight condition by conserving the density and length product. But this scaling starts to break down when the mass flux into the shock layer and radiative heat transfer out of the stream tubes are considered and it may result in the experimental conditions deviating from the flight condition. Consequently, radiative scaling is still not well understood as experimental data is measured around small subscale models or from flight experiments. X3's large size would allow for radiating flow around larger scale models to be measured and increase our understanding of radiative scaling in high enthalpy flows. Before experiments can be conducted, upgrades to X3's driver have to be completed before the high enthalpy test condition can be achieved. This paper outlines the requirements and some preliminary results of the driver upgrade.

Keywords: hypersonics, radiating flows, expansion tubes, scaling

Introduction

When a vehicle returns to Earth from a mission to the Moon, Mars or from deep space, it can have a velocity exceeding 10,000km/s when it enters the atmosphere, which is referred to as a super orbital entry. At these velocities, a shock wave forms in front of the vehicle where the temperatures can reach upwards of 10,000K. Heat is transferred from the shock wave to the vehicle by convection and radiation, and at these conditions, radiation starts to become a significant contributor to the total heat transfer [1].

The internal energy of an atom or molecule depends on the energies associated with electrons spinning in various orbits (electronic) and the translation, rotation and vibration of atoms within molecule. Energy levels within the molecule can change with the absorption or emission of a photon, which is an electromagnetic wave, and radiation is the transfer of heat via electromagnetic waves. If an atom or molecule absorbs a photon its energy level increases and if an atom or molecule emit a photon the internal energy of the particle decreases. The energy levels for electron orbits, molecular vibration or rotation are quantized, this results in energy levels that can only change by discrete amounts. Thus, photons that are absorbed or emitted along with these energy changes will also have discrete amounts of energy [2]. The energy of a photon is defined by the product of Planck's constant ($h = 6.626 \times 10^{-34}$ $[Js]$) and its frequency (ν $[s^{-1}]$), and the wavelength (λ $[m]$) of a photon is defined by the ratio of the speed of light ($c = 2.998 \times 10^{8}$ $[m/s]$) and frequency (eqn 1).

$$\Delta E = h\nu = \frac{hc}{\lambda} \tag{1}$$

The change in energy of an atom or molecule (ΔE $[J]$) is equal to the energy of the photon it absorbs or emits and if the wavelength of the photon is known, the type of energy change and the atom or molecule that is responsible for it can be calculated. Changes in rotational energy require a low amount of energy so the absorbed/emitted photons have longer wavelengths, typically in the far-infrared region, vibration changes absorb/emit photons with wavelengths in the infrared region and electronic changes require the largest energy and absorb/emit photons with the shortest wavelengths in the ultraviolet and visible light regions. There has been recent interest in the vacuum

ultraviolet region ($10nm < \lambda < 200nm$) [3]; which is highly absorbed in the atmosphere but is still a significant contributor to the total radiative heat transfer to the surface of the vehicle [4].
A vehicle entering the atmosphere at super orbital velocities will have temperatures higher than 10,000K in the shock layer. Due to high temperature the gas in the shock layer will emit photons and absorb photons emitted by other atoms or molecules in the flow. If the level of emissions and absorptions in the shock layer are known, the heat transfer to the surface of the re-entry vehicle can be estimated. Anderson [1] estimates the radiative heat transfer to the surface of the vehicle using eqns 2, 3, 4 and 5.

$$\nabla . \mathrm{q_R} = 4\pi \int_0^\infty \kappa_\nu B_\nu d\nu - 2\pi \int_0^\infty \kappa_\nu \int_0^{\tau_{\nu s}} B_\nu(t) \in_1 \times (|\tau_\nu - t|) dt d\nu \quad (2)$$

$$\in_n (t) = \int_0^1 \omega^{n-2} \exp(-t/\omega)\, d\omega \quad (3)$$

$$B_\nu = \frac{2h\nu^3}{[c^2(\exp(h\nu/kT)-1)]} \quad (4)$$

$$\tau_{\nu s} = \int_0^\delta \kappa_\nu(x) dx \quad (5)$$

In Eqn **2**, q_R $[W]$ is the radiative flux to the vehicle stagnation point, κ_ν is the spectral volumetric absorption coefficient, B_ν is the spectral blackbody function, $\tau_{\nu s}$ is the spectral thickness of the shock layer, t is the optical length to some point in the shock layer, $k = 1.38 \times 10^{-23} m^2 kg\, s^{-2}\, K^{-1}$ is the Boltzmann constant and T is the temperature of the gas. These equations can be applied with various radiative transport models, whether the gas is treated as transparent (no absorption), a grey gas (constant absorption coefficient) or as a non-grey gas (varying absorption coefficient with wavelength). Coupling with the flow field also needs to be considered, as radiative transfer from the shock layer out of the area of interest can affect the macroscopic properties of the flow. The level of flow coupling can be estimated by the Goulard number [5], the rule of thumb is if the Goulard number is greater than 0.01, the flow is considered to be strongly coupled [6]. The Goulard number is defined as the ratio of adiabatic radiative energy flux to total energy flux (eqn 6), where ρ_∞ $[kg/m^3]$ and v_∞ $[m/s]$ are the freestream density and velocity respectively.

$$\Gamma = \frac{2q_R}{\frac{1}{2}\rho_\infty v_\infty^3} \quad (6)$$

The level of coupling of the flow becomes important when experimentally measuring the radiative shock layer. Some representative Goulard numbers for various missions are presented in Table 1.

Table 1: Goluard number during re-entry for various missions [6]

Mission	Goulard Number
Moon Return / FIRE II	0.01
Hayabusa	0.013
Jupiter Entry	0.1
Titan Entry	0.4

Previous Work

The FIRE II mission was a flight experiment conducted by NASA on April 14, 1964 with the intent of obtaining heating measurements along a lunar re-entry trajectory [7]. The re-entry vehicle was designed to represent a scaled Apollo re-entry capsule and radiative and convective heat transfer measurements on the surface of the vehicle were made. The results of the surface measurement show that at peak heating, radiative heat transfer accounts for approximately 40% of the total surface heating [8]. The Hayabusa spacecraft was launched by JAXA on 9 May 2003 on the mission to obtain samples from the surface of the asteroid 25142 Itokawa and return the sample to Earth [9]. The Hayabusa capsule re-entered Earth's atmosphere on 13 June 2010 over Australia and spectral observations were made during the capsules descent [10]. Sample results from the observation experiment are shown in Figures 1 and 2. Figure 1 shows the recorded image on the ICCD (intensified charged coupled device) and illustrates the location of the Hayabusa capsule and disintegrating spacecraft bus.

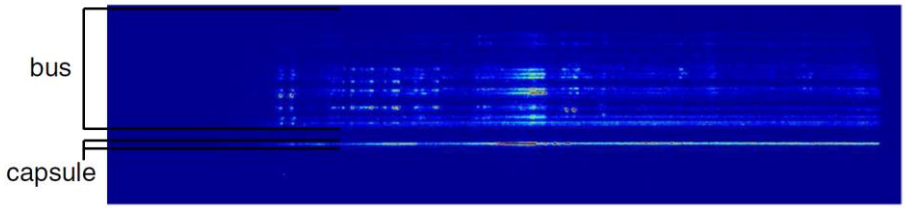

Figure 1: Sample ICCD image of capsule and disintegrating spacecraft bus [10]

Figure 2 presents the spectral irradiance recorded by the image on the ICCD, and the principle species observed are N_2^+ and CN. The CN species arise from Hayabusa's carbon based ablative thermal protection system, with the carbon reacting with dissociated nitrogen. Ca and Ca^+ lines are also identified in the spectra, and aluminium lines were also identified between the two Ca^+ lines although they are not labelled on Figure 2 [10].

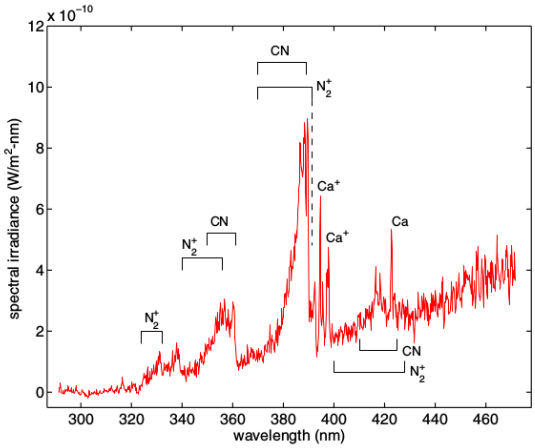

Figure 2: Spectral irradiance of Hayabusa capsule [10]

The gradual increase in intensity in Figure 2 is due to blackbody radiation from the high temperature of the surface of the Hayabusa capsule and the labelled peaks are radiators in the shock layer. Since the observation occurred at a distance of approximately $100km$ from the capsule, the shock layer and vehicle could not be resolved into separate measurements, although the data is still useful as it represents actual flight data and estimates of the vehicle surface temperature can be made.

At UQ, the X2 expansion tube has been used to take radiative measurements of shock layers in front of subscale models in high enthalpy flows [11] for both two dimensional [12], [13] and three dimensional models with and without simulated ablation [14], [15], and for various atmospheric compositions [16], [12], [17], [18]. Experiments have also been conducted in X2 using pre heated models, to simulate the actual vehicle temperature during re-entry [19], [20].

Scaling of Radiating Flows

When scaling a re-entry vehicle down to a size that can be tested in X2, the flow conditions need to be developed such that the properties of the flow are equivalent between the two scenarios. Experiments in X2 have made use of binary scaling which is accomplished by conserving the product of free stream density (ρ $[kg/m^3]$) and a characteristic length (L $[m]$) [12].

When the ρL product is held constant between the actual flight and the subscale model, Reynolds number and viscous effects as well as binary chemical processes are conserved. It has also been shown to reproduce more complex reacting schemes quite accurately [11] and is also scales the convective heat transfer. Binary scaling can conserve radiative transfer from a point in the flow if the gas is optically thin (i.e. no absorption). While this is useful, binary scaling of radiating flows starts to break down when the heat removed from the flow via radiation is considered, as this scales with density times volume (ρL^3) and the mass flux into the shock layer scales with density times area (ρL^2), which results in more heat being lost from the flow around the subscale model than the flight vehicle [11]. If the radiative coupling of the flow is considerable, which can be estimated by the Goulard number, then the flow properties of the subscale flow will start to deviate from that of the flight condition. Mechanisms that violate binary scaling have been outlined in [21] which are: truncation of the nonequilibrium region by the vehicle body; collisional limiting at low densities, where collisions are not sufficient to maintain the

excited states within the gas; energy loss from the gas by radiation cooling is significant; absorption in the gas occurs when it is not optically thin.

Considering experiments in a facility such as X2 and the limitations on the size of model that can be experimented with, only small subscale models can be examined; which drives the necessity to have test flow densities orders of magnitude larger than that of the flight condition, depending on the vehicle of interest. Radiation measurements are made using subscale models, it remains to be validated what the effect of scaling the flow will have on the radiation process and how measurements at the subscale level will differ from modelling at larger scales. The advantage of using X3 is that it will allow for the experimentation of larger scale models and for some vehicles, such as the Hayabusa capsule, may allow for the experimentation of full scale models. While 1:10 model of the Hayabusa capsule has been experimented with in X2 [14], the density in the test flow would be 10 times higher than that of the flight density at the point of interest, and considering the Goulard number from Table 1, the experimental test conditions may have deviated from the flight conditions, although a reasonable representation of the non-equilibrium region and viscous shock layer can still be obtained [6].

These limitations of reproducing the radiative environment in smaller facilities has driven the desire to perform high enthalpy experiments in the larger X3 facility. The larger size of X3 will allow experimental measurements of large scale models (scales up to 1:2) and future developments of a larger nozzle may allow for full scale experiments of smaller re-entry capsules such as a Hayabusa capsule (diameter 400mm [10]) or a Stardust capsule (diameter 811mm [22]). While full scale testing will be able to produce experimental measurements of the actual flight condition without the need to scale the properties of the flow (and will be limited to only a few possible vehicles), experimental results are of more importance as it will allow us to establish the effect of scale on radiating flows.

X3 Expansion Tube

The X3 expansion tube is the world's largest free-piston driver expansion tube and is currently used to generate hypersonic flows for either planetary re-entry or hypersonic air-breathing flight. The expansion tube consists of a high pressure reservoir, compression tube, optional secondary driver (between primary and secondary diaphragm), shock tube (between primary and secondary diaphragm, or between secondary and tertiary if a secondary driver is used), and acceleration tube (remaining downstream section), and a geometric layout is presented in Figure 3. A Mach 10 nozzle is currently installed at the end of the acceleration tube and the facility is able to produce core flows of 200mm in diameter, with steady flows for up to 1ms in duration.

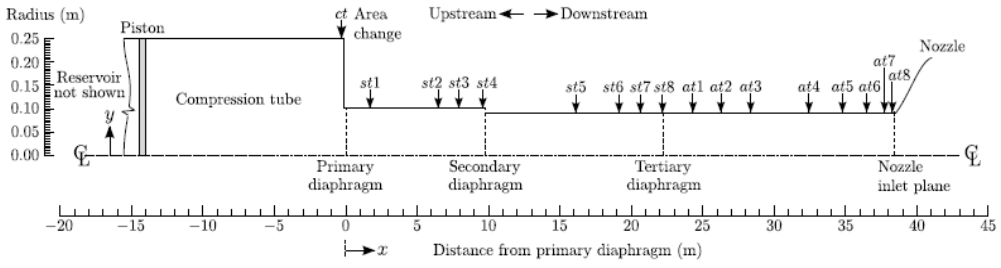

Description	x (m)	y (m)
Piston front face	−14.022	-
Transducer ct	−0.200	-
Driver area change	−0.100	-
Primary diaphragm	0	0.250
Transducer $st1$	1.649	0.100
Transducer $st2$	6.504	0.100
Transducer $st3$	7.955	0.100
Transducer $st4$	9.519	0.100

Description	x (m)	y (m)
Secondary diaphragm	9.772	-
Transducer $st5$	16.123	0.090
Transducer $st6$	19.217	0.090
Transducer $st7$	20.715	0.090
Transducer $st8$	22.207	0.090
Tertiary diaphragm	22.237	-
Transducer $at1$	24.307	0.0913
Transducer $at2$	26.336	0.0913

Description	x (m)	y (m)
Transducer $at3$	28.365	0.0913
Transducer $at4$	32.430	0.0913
Transducer $at5$	34.894	0.0913
Transducer $at6$	36.494	0.0913
Transducer $at7$	38.095	0.0913
Transducer $at8$	38.524	0.0913
Nozzle inlet plane	38.599	-
Nozzle exit plane	41.148	-

Figure 3: Geometric layout of X3 [23]

The current compression tube operates utilising a piston that compresses the driver gas in the compression tube to a high temperature and pressure which then ruptures the primary diaphragm. Three diaphragm thicknesses are typically used: 2mm, 3mm and 4mm which nominally rupture at 17.5MPa, 26.3Mpa and 35.0MPa respectively. Once the primary diaphragm ruptures, the high temperature and pressure gas in the compression tube flows into the next section of the tube generating a strong shock the downstream test gas. This shock compresses the gas in the next section and ruptures the secondary diaphragm. If no secondary driver is used, the shock-processed gas expands into the acceleration tube and through the nozzle generating the desired high pressure condition. The current configuration utilises a 200kg piston and a compression gas composition of 60% helium and 40% argon.

Helium is used as a driver gas since it has a high sound speed which is required to produce a fast shock [24], but a consequence of this is that helium vents into the next section relatively quickly, which can lead to a rapid pressure drop depending on the piston speed at time of rupture. To mitigate this the heavier gas is added to lower the mass flow rate; argon is chosen since it is monatomic and has an equal ratio of specific heats as helium [25].
Recent experiments in X2 have measured the radiation in the shock layer around a 1:5 scale Hayabusa capsule model [26] and it is planned to examine a larger scale Hayabusa model in X3 in the future. Since the configuration of X2 and X3 are similar, and both nozzles have the same area ratio, the enthalpy and velocity of the test flow in X2 can be matched in X3 if the shock speeds in the shock tube and acceleration tube are matched. If the shock speeds are matched, the velocity of the test gas exiting the nozzle will be approximately the same in X3 as it is for X2, although the free stream density will depend on X3's relative driver performance.

Compression Tube

In recent years several upgrades have been made to X3, including upgrading the piston to a single stage piston rather than a two stage piston, modifications to the compression tube and the installation of a Mach 10 nozzle [27]. The current compression tube employs a 200kg piston which compresses a gas composed of 60% helium and 40% argon. Preliminary calculations have been done simulating the facility in PITOT [28], [29], which uses isentropic and compressible gas processes to simulate the conditions in the expansion tube. It utilizes NASA's Chemical Equilibrium with Applications (CEA) [30] to account for high temperature gas effects. PITOT assumes a constant driver temperature and pressure and ignores piston dynamics and transient variations in these properties. These assumptions can be used on X3 since the 'tuned' driver will keep these properties at approximately constant values for the relevant timescales. Regardless, PITOT can still calculate conditions in the expansion tube with reasonable accuracy, except in the acceleration tube where boundary layer and low density effects cause the results to deviate from the experimental condition [29]. Results from PITOT have found that the current driver operating condition does not have enough performance to match the shock speeds used in X2, the results of which are presented in Table 2**,** which conclude that the current driver configuration does not have the performance to match the shock speeds in X2.

Table 2: Results from a PITOT simulation of X3 with the current compression tube arrangement.

Driver Composition	Shock Tube Fill Pressure (Pa)	Primary Shock Speed (m/s)
X2 Driver	-	4750
60% helium; 20% argon	151	3822.0
	201	3763.9
	251	3717.5
	301	3679.5

To increase the sound speed, either the weight of the compression gas can be reduced, by having a higher ratio of helium, or the compression ratio of the compression tube can be increased. Increasing the compression ratio is limited by the length of the compression tube, for a constant driver fill pressures, and the maximum allowable pressure in the reservoir. Increasing the sound speed of the driver gas is limited by the duration that the high pressure is maintained after diaphragm rupture, which is ultimately limited by the maximum piston speed. If the piston velocity at diaphragm rupture is relatively low then the driver behaves like it has a constant volume and as gas vents through the tube the high pressure condition is lost. Due to the length of X3, not maintaining the pressure after diaphragm rupture significantly decreases the performance of the tube and may cause interference with downstream flow process interrupting the test time [31]. Stalker [32] proposed 'tuning' the operation of the piston to maintain the pressure in the compression tube after diaphragm rupture. The 'tuned' driver is achieved by accelerating the piston to higher velocities so the diaphragm ruptures when the piston still has high velocity, and this will allow the displacement of the piston to compensate the flow rate of the driver gas through the expansion tube, which can maintain the high pressure condition. A pressure trace taken from X3's compression tube is shown in Figure 4, the rupture pressure for the experiment is nominally 17.5MPa, and the high pressure after diaphragm rupture is only maintained for a short duration of time.

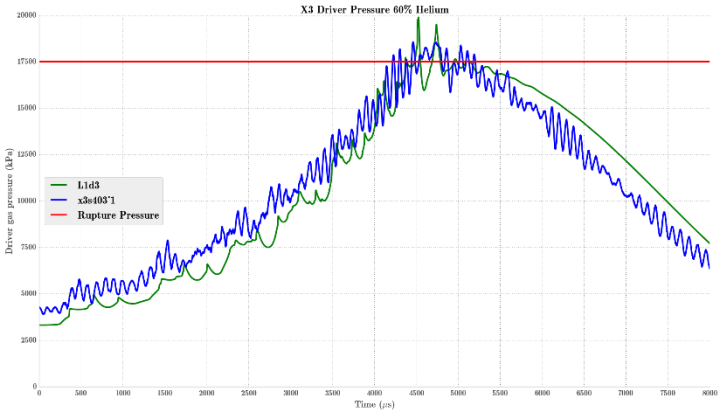

Figure 4: Experimental pressure trace taken from X3's compression tube and compared to numerical simulations using L1d. The red line shows the rupture pressure.

Piston

To match the flow rate of the driver gas, the piston will have to operate at speeds around 250m/s [23], and this acceleration and deceleration from this velocity (to avoid the piston striking the end of the compression tube) has to occur within the compression tube which has a length of approximately 14m. Since the reservoir pressure is limited, to achieve the high velocities required a piston with low mass is required. A new lightweight piston weighing 101.8kg has been designed for use in X3's compression tube [23] and is shown in Figure 5. The piston was designed for the lowest mass possible which still maintaining structural integrity during normal operation.

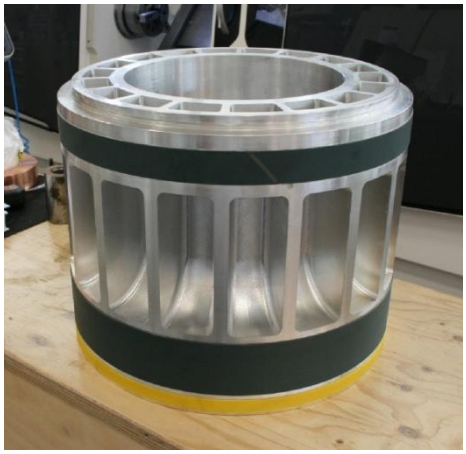

Figure 5: New lightweight piston for X3 [23]

The new lightweight piston has previously been installed in X3 [23] although no experiments have been conducted with it. Blank off tests were performed for the condition to be used with a 2mm diaphragm and a 100% argon driver. The results of the blank off test and numerical simulations using L1d [32], which is a program developed for the one dimensional simulation of transient-flow facilities and is also capable of modelling the motion of the piston, are shown in figure 6. The reservoir fill pressure used to generate the plots in figure 6 was 8.4Mpa and the maximum piston velocity produced was approximately 200m/s, which is considerably lower than the maximum velocities in figure 14. To account for his, reservoir extension has been designed, which serves the purpose of increasing the reservoir volume. This will effectively increase the performance of the reservoir and allow the piston to achieve higher velocities for the same reservoir fill pressure. An image of the reservoir extension is shown in figure 7.

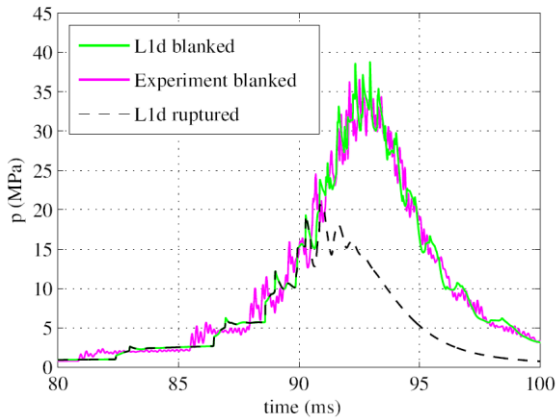

Figure 6: Experimental blank of test for the new lightweight piston (purple) compared with numerical blank off test in L1d (green). A numerical simulation conducted in L1d with a rupturing diaphragm is represented by the dashed line [23].

Figure 7: X3 reservoir extension.

Analysis using the method outlined by Stalker [31] provides an estimate for the 'tuned' piston mass for compression tube length and driver operating conditions. The analysis sets the kinetic energy of the piston to be equal to the work required to vent the remaining driver gas at some point after diaphragm rupture, denoted by the subscript r. The relation used is defined in eqn 7, where $p_{D,r}$ $[Pa]$ and $p_{A,r}$ $[Pa]$ are the driver and reservoir gas fill pressurse respectively, V_r $[m/s]$ is the volume in the remaining volume in the compression tube, k is a constant ($= 1/2$ for kinetic energy), m_p $[kg]$ is the mass of the piston, A is the cross sectional area of the compression tube and U_r is the velocity of the piston.

$$\left(p_{D,r} - p_{A,r}\right)V_r = k\frac{m_p}{A}AU_r^2 \tag{7}$$

Stalker sets k=1 to ensure that the piston stops before striking the end of the compression tube. The subsequent analysis provides the following estimates for piston mass displayed in figure 8, 9 and 10, figure 8 models the gas venting directly into the shock tube without any restriction. Figures 9 and 10 include orifice plates with diameters of 175mm and 154mm which serve the purpose of restricting the flow of the driver gas out of the compression tube. X3's compression tube is approximately 14m long and operates at a nominal compression ratio of approximately λ=40, and for that compression ratio the analysis suggest that the 101.8kg lightweight piston is too heavy to be used with any of the nominal driver compositions. As the orifice diameter decreases, and the flow rate of the driver gas is restricted, the requirements for a light piston start to relax because the required velocity to match the driver gas flow decreases. In figure 10 it can be seen that the lightweight piston mass of 101.8kg may be suitable for an 80% helium driver at a compression ratio of 40 or a 100% helium driver operating at a compression ratio of 20.

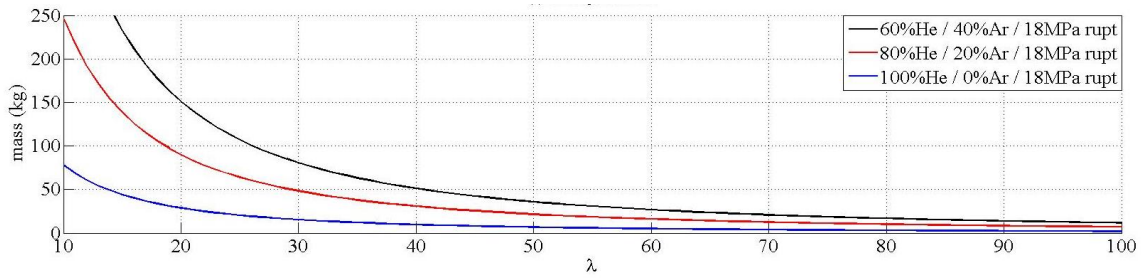

Figure 8: Estimates of 'tuned' piston mass with no orifice plate installed.

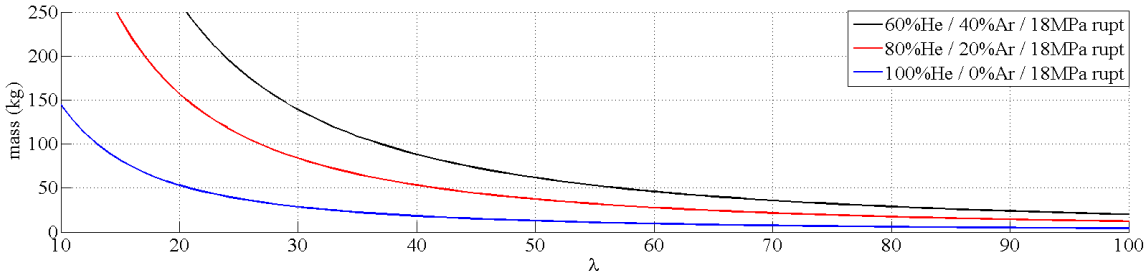

Figure 9: Estimates of 'tuned' piston mass with a 175mm diameter orifice plate installed.

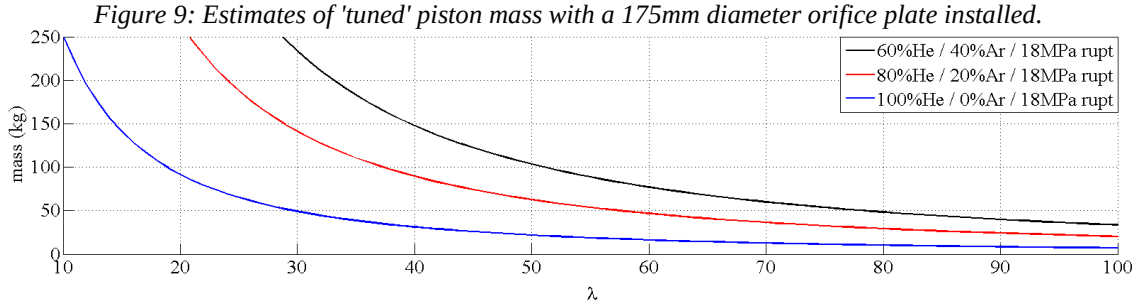

Figure 10: Estimates of 'tuned' piston mass with a 154mm orifice plate installed.

While figures 8 to 10 give an idea of what the piston mass should be, the piston trajectory can be modelled more accurately using the methodology outlined by Hornung [24]. Hornung makes the assumption that reservoir behind the piston has infinite extent, so wave processes in the reservoir can be ignored. Since the driver gas typically has high sound speed and the piston velocity is very subsonic in the helium, the pressure in the driver gas can be assumed to be spatially uniform and undergoing an adiabatic compression [24]. With these assumptions, the motion of the piston with mass M [kg] in a compression tube of length L [m] and diameter D [m] before diaphragm rupture is defined by eqn 8. x [m] is the piston's location along the compression tube; u [m/s] is the piston's velocity; p_{R_0} $[Pa]$ and p_{D_0} $[Pa]$ are the initial pressures in the reservoir and compression tube respectively; γ_R $[-]$ and γ_D $[-]$ are the ratio of specific heats of the reservoir and driver gasses and a_0 $[m/s]$ is the initial sound speed of the reservoir gas.

$$-M\frac{d^2x}{dt^2} = \frac{\pi D^4}{4}\left\{p_{R_0}\left(1-\frac{\gamma_R-1}{2}\frac{u}{a_0}\right)^{\frac{2\gamma_R}{\gamma_R-1}} - p_{D_0}\left(\frac{L}{x}\right)^{\gamma_D}\right\} \tag{8}$$

After diaphragm rupture, the mass flow of the driver gas into the shock tube needs to be accounted for. The rate of change of mass in the compression tube is defined in eqn 9.

$$\frac{dm}{dt} = -\frac{\sqrt{\pi\gamma_D}}{2}\left(\frac{2}{\gamma_D+1}\right)^{\frac{\gamma_D+1}{2\gamma_D+1}}\frac{d^2}{D^2}\sqrt{p_{D_r}}\left(\frac{x_r}{m_r}\right)^{\frac{\gamma_D}{2}}\left(\frac{m}{x}\right)^{\frac{\gamma_D+1}{2}} \tag{9}$$

In eqn **9**: m $[kg]$ is the mass of the driver gas; d $[m]$ is the diameter of the orifice connecting the compression tube to the shock tube; p_{D_r} $[Pa]$ is the diaphragm rupture pressure; x_r $[m]$ and m_r $[kg]$ are the location of the piston and mass of helium in the compression tube at the time of rupture. The mass flow of the driver gas and the pressures in front of and behind the piston can be used to model the motion of the piston from diaphragm rupture until it

strikes the end of the compression tube. The motion of the piston is shown in eqn 10 where $p_R[Pa]$ is the pressure upstream of the piston, which assumes a shock has been generated that is strong enough to stagnate the gas if the piston suddenly stops.

$$\frac{d^2x}{dt^2} = \left[p_{D_r}\left(\frac{x_r}{m_r}\right)^{\gamma_D}\left(\frac{m}{x}\right)^{\gamma_D} - p_R\right]\frac{\pi D^2}{4M} \tag{10}$$

Eqns 8 and 10 model the piston motion from launch until it strikes the end of the compression tube. Once the motion has been established different initial pressures and compositions of reservoir and driver gasses can be simulated to examine the effect they have on the motion of the piston. To 'tune' the driver, the piston is required to have a velocity high enough to match the mass flow rate of the driver gas and Stalker [31] proposed to idea to operate faster than the 'tuned' velocity at diaphragm rupture to increase the pressure of the driver gas beyond the diaphragm rupture pressure, essentially over-driving the piston. Itoh [34] characterised the over drive parameter β as the ratio of the piston velocity and the required piston velocity to match the mass flow rate of the driver gas (eqn 11). The effects of various values of β is shown in figure 11; it has been found that an over-pressure of the driver gas of 10% is permitted to keep the pressure behind the primary shock wave nearly constant which corresponds to a value of $\beta \approx 1.2 - 1.6$.

$$\beta = \frac{u_{rupt}}{U_{ref}} \tag{10}$$

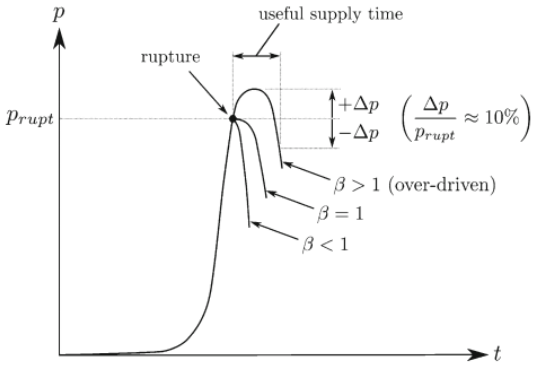

Figure 11: Effect of changing the over drive parameter has on the pressure in the compression tube [30]

For a value of $\beta = 1$ the motion of the piston matches the mass flow and the pressure in the compression tube is maintained before decreasing since the piston is accelerating and will not continue to match the flow rate of the driver gas. When $\beta < 1$ the pressure of the driver gas as the volume of the driver gas approaches a constant volume. For $\beta > 1$ the pressure will increase momentarily before the pressure of the driver gas drops after the piston continues to decelerate. Utilising the 10% limit on the driver pressure, the time of useful driver pressure can be found by measuring the time when the driver pressure is $\pm 10\%$ of the diaphragm rupture pressure. Additionally to prevent damage to the facility, it is important that the piston does not strike the end of the compression tube with any significant velocity. Various piston trajectories are displayed in figure 12, where ω is the work the driver gas does on the piston and ω_S is the kinetic energy of the piston, and u_m is the velocity of the piston when it has zero acceleration.

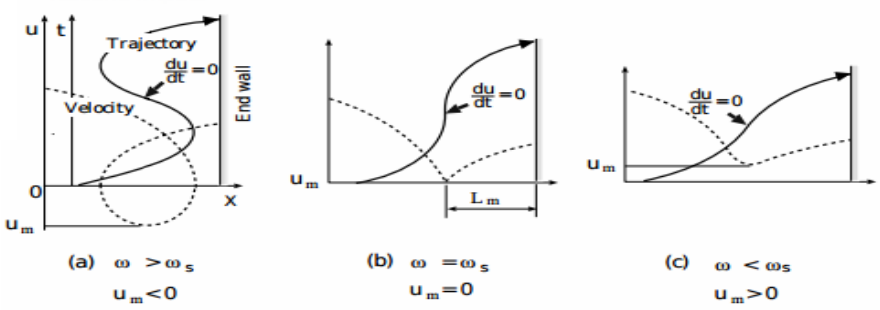

Figure 12: Possible piston trajectories after diaphragm rupture \cite{itoh1998improvemnt}

In figure 12: (a) is if the work done to the piston is greater than the piston's kinetic energy so the driver gas begins to push the piston back upstream before the piston strikes the end wall; (c) is if the kinetic energy of the piston is greater than the work done and the piston directly strikes the end of the wall; (b) has the kinetic energy of the piston and the work done be the driver gas equal, so the piston momentarily comes to rest at some point before the end of the compression tube. In figure 12 (b) the piston can be caught at the location where it has zero velocity by using a buffer on the end of the compression tube. This concept is currently in use for a 'tuned' driver on X2 [30] and will be used for the 'tuned' X3 driver.

Preliminary Results

The motion of the piston was simulated using eqns 8 and 10 the driver composition of 80% helium and 20% argon. Because of the assumptions of the infinite reservoir, the motion of the piston from rest to its maximum velocity can be disregarded as it does not accurately depict the actual reservoir on X3. Once the piston reaches its maximum velocity, the driver gas has a significantly larger effect on the motion than the reservoir gas, so the motion of the piston from this point to the end of its stroke is modelled reasonably accurately to get an initial estimate of what the initial driver gas pressure will be and what some key parameters of the piston motion are. While the diameter of the shock tube is 200mm, simulations have also been run using an orifice plate of 154mm to restrict the flow rate of the driver gas into the shock tube. Key parameters from each simulated trajectory using the new lightweight piston mass are shown in table 3 and it can be seen for the larger orifice diameter that the required piston velocity increases by a substantial amount, as well as the initial pressures in the reservoir and compression tube. The orifice diameter of 200mm has not been included in table 3 as no solution could be found with reasonable fill pressures that satisfied the 10% pressure overshoot and having a point of zero velocity. The trajectory for each fill pressure in table 3 is also shown in figure 13.

Table 3: Piston motion calculated using Hornung's analysis (eqn 8 and eqn 10)

Reservoir Pressure (MPa)	Compression Tube Pressure (kPa)	Driver Gas Composition	Orifice Diameter (mm)	Maximum Piston Velocity (m/s)	Piston Rupture Velocity (m/s)	Maximum Driver Pressure (MPa)
2.73	89.8	80%He; 20%Ar	154	214.3	138.6	19.25
4.46	182.0	80%He, 20%Ar	175	244.2	156.2	19.25

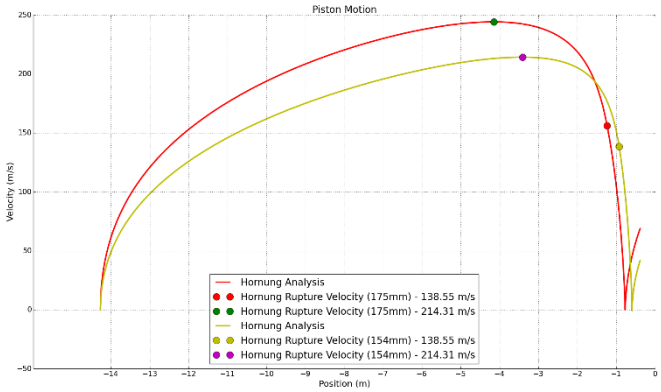

Figure 13: Piston trajectories for the conditions outlined in table 3. The diaphragm is located at x=0m

Figure 13 shows the requirement for an increases in piston velocity to match the flow rate of the gas for larger orifice diameters. For the 175mm orifice, the reservoir pressure must be higher since the piston needs to be accelerated to higher velocities and as a consequence the compression tube fill pressure must also be higher to decelerate the piston and prevent it striking the end of the tube. The motion of the piston before the maximum velocity is determined largely by the reservoir fill pressure, and the higher reservoir pressure results in the piston reaching a higher maximum velocity and sooner than the lower fill pressure. Once the maximum velocity is reached the motion becomes largely dependent on the driver gas in front of the piston, and since the larger orifice has a larger flow rate more driver gas is required to decelerate the piston.

The motion of the piston with a 154mm orifice plate was also simulated using L1d3. An important point to note here is that the reservoir of X3 is currently located under the compression tube, so the reservoir gas needs to travel around a 90 degree bend to act on the piston. While L1d3 can account for area change, it cannot accurately model

the geometry of the three dimensional bend that connects X3's reservoir and compression tube. Instead, L1d3 incorporates a loss factor, which while isn't based off any physics involved in the operation of the expansion tube, it can accurately account for losses in various locations once the numerical results are matched with experimental results. For the piston this will be done by conducting blank off tests like those in figure 6. At the time of writing, blank off tests with the new piston and reservoir have not been conducted, but the numerical analysis still can still be used to compare the that of figure 12 although the reservoir pressure used will not be accurate. The numerical simulation was done with the orifice plate accounted for, so the driver gas is vented through a diameter of 154mm, rather than the shock tube diameter of 200mm.

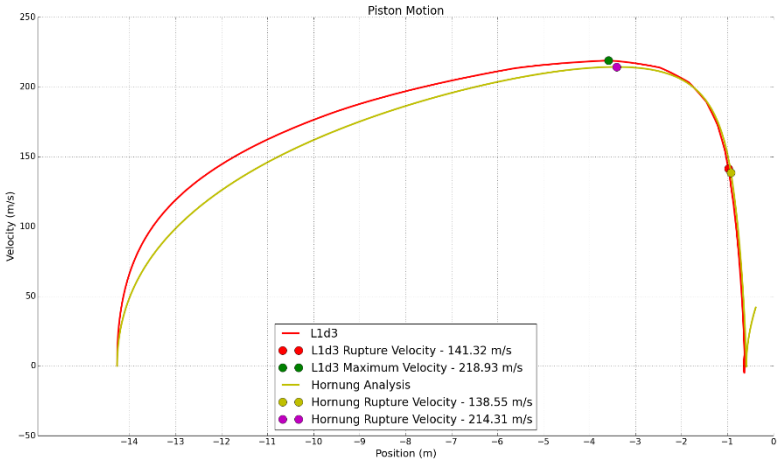

Figure 14: Piston motion modelled using Hornung's analysis and L1d3 using an orifice diameter of 154mm. The diaphragm is located at a position of x=0m.

The reservoir fill pressure used for the L1d3 simulation in figure 14 was 7.5MPa compared to the 2.73MPa used for the ideal simulation and the same driver fill pressure was used for each case. Figure 14 shows that while the initial trajectory differs shortly after launch the location and magnitude of the maximum and rupture velocities are similar between the two simulations. While the ideal analysis has been iterated to get a perfect inflection point, the L1d3 simulation has the piston travel back upstream slightly before continuing downstream to the end of the tube. Disregarding these exceptions, which will be accounted for later, the motion of the piston after it reaches its maximum velocity is consistent between the two simulation methods. Ultimately it is the pressure in the compression tube which is of interest, and results from the ideal analysis are shown in figure 15 for both the 154mm and 175mm orifice plates. The pressure in the compression tube for both orifice plates have similar shapes and also have similar durations where the pressure us within the acceptable range for assuming a constant driver pressure, which is marked on each curve in figure 15. Since the performance of each orifice is similar, although using different fill pressures which may be limited the pressure capacity of the tube since the actual fill pressure for the reservoir is likely to be higher than that used in the ideal analysis. There are also implications of using different sized orifice plates on the performance downstream of the driver, as a smaller restriction results in a larger expanded mach number in the shock tube which typically has a negative effect on the downstream performance [34].

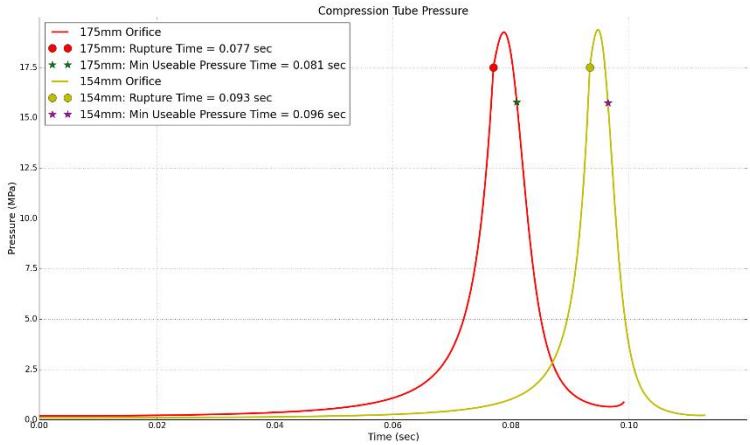

Figure 15: Pressure in the compression tube during the piston stroke using the ideal analysis for both the 154mm orifice (yellow) and the 175mm orifice (red).

While the ideal analysis gives a reasonable estimate to the piston motion, especially after the point of diaphragm rupture when compared to L1d3, experimental results will be needed to accurately model the motion of the piston from launch. Blank off tests using the new lightweight piston and reservoir extension are required to accurately quantify the loss coefficients in L1d3. Another benefit to performing the blank off shots will be to match the current driver used with the new hardware. This will be done by firing blank off shots with the current piston, current piston and reservoir extension, and lightweight piston and reservoir extension. If the pressure traces are matched across the three combinations of hardware, the condition used in X3 will be conserved, and it is intended the current piston will still be used in the future, so having blank off data with the current piston and reservoir extension will be beneficial. Once the blank off tests are complete and the losses characterised in L1d3, the reservoir and driver pressures can be calculated to produce a 'tuned' free piston driver.

Conclusion

To simulate the flight conditions that a vehicle experiences during re-entry several upgrades to the X3 expansion tube are required. The study of high enthalpy flows in X3 will allow for larger scale models, or potentially full scale models, examined and the radiating flow around the model measured. This will further increase our understanding of radiative flows and how they scale as currently experimental results are limited to small sub scale models or data from flight experiments and observations.

The current free-piston driver does not have enough performance to produce a strong enough shock in the shock tube and consequently through the acceleration tube. To improve the performance of the driver the sound speed of the driver gas needs to be increased, which means a lighter gas has to be used and the corresponds to a higher percentage of helium than what is currently in use (60% helium 40% argon). By increasing the helium composition the driver gas vents into the shock tube faster which will require the piston trajectory to be recalculated to maintain the 'tuned' driver. A new lightweight piston and reservoir extension have been designed as part of X3's driver upgrade, and the new hardware will enable the piston to be driver at higher speeds than the current piston and match the flow of the driver gas out of the compression tube. Once the new hardware has been installed, the driver operating conditions can be developed using experimental data from blank off tests and correlating this with numerical analysis using L1d3 to finalise new fill pressures and compositions for the reservoir and compression tube for various diaphragm thicknesses. This will eventually lead to the development of new operating conditions in X3 that will be used to examine the high enthalpy conditions experienced during super orbital re-entry.

Acknowledgements

The authors wish to thank: Mr F. De Beurs for technical support; The Australian Research Council for support and funding; The Queensland Smart State Research Facilities Fund 2005 for support and funding and The Australian Space Research Program.

References

1. Anderson, Jr., J. D. (1969), 'An engineering survey of radiating shock layers.', *AIAA Journal* **7**(9), 1665--1675.

2. Modest, M. F. (2013), *Radiative heat transfer*, Academic press.

3. Sheikh, U. (2014), 'Re-entry radiation aerothermodynamics in the vacuum ultraviolet'

4. Bose, D.; McCorkle, E.; Thompson, C.; Bogdanoff, D.; Prabhu, D.; Allen, G. & Grinstead, J. (2008), 'Analysis and model validation of shock layer radiation in air', *VKI LS Course on hypersonic entry and cruise vehicles, Palo Alto, California, USA*.

5. Goulard, R. (1961), 'The coupling of radiation and convection in detached shock layers', *Journal of Quantitative Spectroscopy and Radiative Transfer* **1**(3), 249--257.

6. Leyland, P.; McIntyre, T.; Morgan, R.; Jacobs, P.; Zander, F.; Sheikh, U.; Eichmann, T.; Fahy, E.; Joshi, O.; Duffa, G. & others (2013), Radiation-Ablation Coupling for Capsule Reentry Heating via Simulation and Expansion Tube Investigations, *in* 'Proceedings of the 5th European Conference for Aeronautics and Space Sciences (EUCASS)'.

7. Cauchon, D. L. (1967), 'Radiative heating results from the FIRE II flight experiment at a reentry velocity of 11.4 kilometers per second', *NASA TM X-1402*.

8. Cornette, E. (1966), 'Forebody temperatures and calorimeter heaheat rates measured diring project Fire II reentry at 11.35 kilometers per second.', *Technical Momorandum TM X-1305, NASA Langley Research Center*.

9. Kawaguchi, Jun'ichiro, Kuninori Uesugi, and Akira Fujiwara. "The MUSES-C mission for the sample and return—its technology development status and readiness." *Acta Astronautica* 52.2 (2003): 117-123.

10. Buttsworth, D.; Morgan, R. & Jenniskens, P. (2013), 'Near-Ultraviolet Emission Spectroscopy of the Hayabusa Reentry', *Journal of Spacecraft and Rockets* **50**(6), 1109--1120.

11. Morgan, R.; McIntyre, T.; Buttsworth, D.; Jacobs, P.; Potter, D.; Brandis, A.; Gollan, R.; Jacobs, C.; Capra, B.; McGilvray, M. & Eichmann, T. (2008), Impulse facilities for the simulation of hypersonic radiating flows, *in* 'AIAA 38th Fluid Dynamics Conference and Exhibit'.

12. de Crombrugghe, G.; Gildfind, D.; Zander, F.; McIntyre, T. & Morgan, R. (2014), Design of Test Flows to Investigate Binary Scaling in High Enthalpy CO2 – N2 Mixtures, *in* '19th Australasian Fluid Mechanics Conference'.

13. Sheikh, U.; Morgan, R. & McIntyre, T. (in press 2015), 'Vacuum Ultraviolet Spectral Measurements for Superorbital Earth Entry in X2 Expansion Tube', *AIAA Journal*.

14. Buttsworth, D.; D'Souza, M.; Potter, D.; Eichmann, T.; Mudford, N.; McGilvray, M.; McIntyre, T. J.; Jacobs, P. & Morgan, R. (2010), *Expansion tunnel radiation experiments to support hayabusa re-entry observations*.

15. Fahy, E.; Morgan, R.; McIntyre, T. & Buttsworth, D. (2014), Scaled Hayabusa Experiments in the X2 Expansion Tube, *in* '6th International Workshop on Radiation of High Temperature Gases in Atmospheric Entry'.

16. Eichmann, T. (2012), 'Radiation Measurements in a Simulated Mars Atmosphere', PhD thesis, the University of Queensland.

17. Porat, H.; Sheikh, U.; Eichmann, T.; McIntyre, T. & Morgan, R. (2013), Vacuum Ultraviolet and Ultraviolet Emission Spectroscopy Measurements for Titan and Mars Atmospheric Entry Conditions, *in* '44th AIAA Thermophysics Conference'.

18. James, C.; Gildfind, D.; Morgan, R.; Lewis, S. & McIntyre, T. (2015), Simulating Gas Giant Entry with Increased Helium Diluent in an Expansion Tube, *in* '30th International Symposium on Shock Waves'.

19. Zander, F.; Morgan, R.; Sheikh, U.; Buttsworth, D. & Teakle, P. (2013), 'Hot-Wall Reentry Testing in Hypersonic Impulse Facilities', *AIAA Journal* **51**, 476-484.

20. Lewis, S. W.; Morgan, R. G.; McIntyre, T. J.; Alba, C. R. & Greendyke, R. G. (in press 2015), 'Expansion Tunnel Experiments of Earth Re-entry Flow with Surface Ablation', *Journal of Spacecraft and Rockets*.

21. Sharma, S. P. & Whiting, E. E. (1996), 'Modeling of nonequilibrium radiation phenomena - An assessment', *Journal of Thermophysics and Heat Transfer* **10**(3), 385--396.

22. Desai, P. N.; Lyons, D. T.; Tooley, J. & Kangas, J. (2008), 'Entry, Descent, and Landing Operations Analysis for the Stardust Entry Capsule', *Journal of Spacecraft and Rockets* **45**(6), 1262--1268.

23. Gildfind, D.; Morgan, R. & Sancho, J. (2014), Design and commissioning of a new lightweight piston for the X3 Expansion Tube, *in* '29th International Symposium on Shock Waves'.

24. Hornung, H. G. (1988), 'The piston motion in a free-piston driver for shock tubes and tunnels', *GALCIT Report FM*, 88--1.

25. Jacobs, P. A., et al. "Use of argon-helium driver-gas mixtures in the T4 shock tunnel." *Shock Waves@ Marseille I*. Springer Berlin Heidelberg, 1995. 263-268.

26. Fahy, E., Personal Communication.

27. Dann, A.; Morgan, R.; Gildfind, D.; Jacobs, P.; McGilvray, M. & Zander, F. (2012), Upgrade of the X3 Super-orbital Expansion Tube, *in* '18th Australasian Fluid Mechanics Conference'.

28. James, C.; Gildfind, D.; Morgan, R.; Jacobs, P. & Zander, F. (2013), Designing and Simulating High Enthalpy Expansion Tube Conditions, *in* '2013 Asia-Pacific International Symposium on Aerospace Technology'.

29. James, C.; Gildfind, D.; Morgan, R.; Lewis, S.; Fahy, E. & McIntyre, T. (2015), On the Current Limits of Simulating Gas Giant Entry Flows in an Expansion Tube, *in* '30th International Symposium on Shock Waves'.

30. McBride, D. & Gordan, G. (1996), *Computer Program for Calculations of Complex Chemical Equilibrium Compositions and Applications II. Users Manual and Program Description*, Nasa Lewis Research Center, Cleveland, OH, U.S.A..

31. Gildfind, D.; Morgan, R.; McGilvray, M.; Jacobs, P.; Stalker, R. & Eichmann, T. (2011), 'Free-piston driver optimisation for simulation of high Mach number scramjet flow conditions', *Shock Waves* **21**(6), 559--572.

32. Stalker, R. (1967), 'A study of the free-piston shock tunnel.', *AIAA Journal* **5**(12), 2160--2165.

33. Jacobs, P. A. (1998), 'Shock tube modelling with L1d'.

34. Itoh, K.; Ueda, S.; Komuro, T.; Sato, K.; Takahashi, M.; Miyajima, H.; Tanno, H. & Muramoto, H. (1998), 'Improvement of a free piston driver for a high-enthalpy shock tunnel', *Shock Waves* **8**(4), 215--233.

35. Gildfind, D.; James, C. & Morgan, R. (2015), 'Free-piston driver performance characterisation using experimental shock speeds through helium', *Shock Waves* **25**(2), 169-176.